PNAS
www.pnas.org

Main Manuscript for

Photosynthesis tunes quantum mechanical mixing of electronic and vibrational states to steer exciton energy transfer

Jacob S. Higgins,[1] Lawson T. Lloyd,[1] Sara H. Sohail,[1,5] Marco A. Allodi,[1] John P. Otto,[1] Rafael G. Saer,[3,4] Ryan E. Wood,[1] Sara C. Massey,[1,6] Po-Chieh Ting,[1] Robert E. Blankenship,[2,3,4] and Gregory S. Engel[1,*]

[1] Department of Chemistry, The Institute for Biophysical Dynamics, The James Franck Institute, The University of Chicago, Chicago, Illinois 60637, United States

[2] Department of Chemistry, [3]Department of Biology, and [4]The Photosynthetic Antenna Research Center, Washington University in St. Louis, St. Louis, Missouri 63130, United States

[5] Present address: Laboratory of Chemical Physics, National Institute of Diabetes, and Digestive, and Kidney Diseases, National Institutes of Health, Bethesda, Maryland 20892, United States

[6] Present address: Department of Chemistry and Biochemistry, Southwestern University, Georgetown, Texas 78626, United States

* Corresponding author. **Email:** gsengel@uchicago.edu

Classification
Physical Sciences: Chemistry; Biological Sciences: Plant Biology

Keywords
Quantum effects in Biology, ultrafast spectroscopy, photosynthesis, excitonic energy transfer, vibronic coupling

Author Contributions
J.S.H., R.E.W., S.C.M., P-C.T., L.T.L., S.H.S., M.A.A., and J.P.O. performed the experiments. J.S.H., L.T.L., S.H.S., M.A.A., and J.P.O. analyzed the data. R.G.S. and R.E.B. isolated the samples. All authors wrote the manuscript. R.E.B. and G.S.E. designed and oversaw the experiments.

This PDF file includes:
Main Text
Figures 1 to 3
Table 1

Abstract

Photosynthetic species evolved to protect their light-harvesting apparatus from photoxidative damage driven by intracellular redox conditions or environmental conditions (1, 2). The Fenna-Matthews-Olson (FMO) pigment-protein complex from green sulfur bacteria exhibits redox-dependent quenching behavior partially due to two internal cysteine residues(3). Here, we show evidence that a photosynthetic complex exploits the quantum mechanics of vibronic mixing to activate an oxidative photoprotective mechanism. We use two-dimensional electronic spectroscopy (2DES) to capture energy transfer dynamics in wild-type and cysteine-deficient FMO mutant proteins under both reducing and oxidizing conditions. Under reducing conditions, we find equal energy transfer through the exciton 4-1 and 4-2-1 pathways because the exciton 4-1 energy gap is vibronically coupled with a bacteriochlorophyll-*a* vibrational mode. Under oxidizing conditions, however, the resonance of the exciton 4-1 energy gap is detuned from the vibrational mode, causing excitons to preferentially steer through the indirect 4-2-1 pathway to increase the likelihood of exciton quenching. We use a Redfield model to show that the complex achieves this effect by tuning the site III energy via the redox state of its internal cysteine residues. This result shows how pigment-protein complexes exploit the quantum mechanics of vibronic coupling to steer energy transfer.

Significance Statement

Photosynthetic light harvesting antennae transfer energy toward reaction centers with high efficiency, but in high light or oxidative environments, the antennae divert energy to protect the photosynthetic apparatus. For a decade, quantum effects driven by vibronic coupling, where electronic and vibrational states couple, have been suggested to explain the energy transfer efficiency, but questions remain whether quantum effects are merely consequences of molecular systems. Here, we show evidence that biology tunes inter-pigment vibronic coupling, indicating that the quantum mechanism is operative in the efficient transfer regime and exploited by evolution for photoprotection. Specifically, the FMO complex uses redox-active cysteine residues to tune the resonance between its excitons and a pigment vibration to steer excess excitation toward a quenching site.

Main Text

Introduction

Photosynthetic organisms convert solar photons into chemical energy by taking advantage of the quantum mechanical nature of their molecular systems and the chemistry of their environment(1, 4-6). Antenna complexes, composed of one or more pigment-protein complexes, facilitate the first steps in the photosynthesis process: They absorb photons and determine which proportion of excitations to move to reaction centers, where charge separation occurs(6). In oxic environments, excitations can generate highly reactive singlet oxygen species. These pigment-protein complexes can quench excess excitations in these environments with molecular moieties such as quinones and cysteine residues(1, 7, 8).

The FMO complex, a trimer of pigment-protein complexes found in the green sulfur bacterium *Chlorobium tepidum* (9), has emerged as a model system to study the photophysical properties of photosynthetic antenna complexes (3, 10-19). Each subunit in the FMO complex contains eight bacteriochlorophyll-*a* site molecules (PDB: 3ENI) that are coupled to form a basis of eight partially-delocalized excited states called excitons (**Figure 1**) (20-23). Previous experiments on FMO have observed the presence of long-lived coherences in nonlinear spectroscopic signals at both cryogenic and physiological temperatures(11, 13). The coherent signals are thought to arise from some combination of electronic(24-26), vibrational(16-18), and vibronic(27) coherences in the system(28-30). One previous study reported that the coherent signals in FMO remain unchanged upon mutagenesis of the protein, suggesting that the signals are ground state vibrational coherences(17). Others discuss the role of vibronic coupling, where electronic and nuclear degrees of freedom become coupled (29). Other dimeric model systems have demonstrated the regimes in which these vibronically coupled states produce coherent or incoherent transport and vibronic coherences(31-33). Recent spectroscopic data has suggested that vibronic coupling plays a role in driving efficient energy transfer through photosynthetic complexes(27, 31, 33, 34), but to date there is no direct experimental evidence suggesting that biological systems use vibronic coupling as part of their biological function.

It has been shown that redox conditions affect excited state properties in pigment-protein complexes, yet little is known about the underlying microscopic mechanisms for these effects(1, 3). Many commonly studied light-harvesting complexes – including the FMO complex(20), light-harvesting complex 2 (LH2)(35), the PC645 phycobiliprotein(36), and the cyanobacterial antenna complex isiA(37) – contain redox-active cysteine residues in close proximity to their chromophores. As the natural low light environment of *C. tepidum* does not necessitate photoprotective responses to light quantity and quality, its primary photoprotective mechanism concerns its response to oxidative stress. *C. tepidum* is an obligate anaerobe, but the presence of many active anoxygenic genes such as *sodB* for superoxide dismutase and *roo* for rubredoxin oxygen oxidoreductase (38) suggests that it is frequently exposed to molecular oxygen(8, 39). Using time-resolved fluorescence measurements, Orf *et al*. demonstrated that two cysteine residues in the FMO complex, C49 and C353, quench excitons under oxidizing conditions(1), which could protect the excitation from generating reactive oxygen species(8, 40-42). In two-dimensional electronic spectroscopy (2DES) experiments, Allodi *et al*. showed that redox conditions in both the wild-type and C49A/C353A double mutant proteins affect the ultrafast dynamics through the FMO complex(3, 43). The recent discovery that many proteins across the evolutionary landscape possess chains of tryptophan and tyrosine residues provides evidence that these redox-active residues may link the internal protein behavior with the chemistry of the surrounding environment(41, 43).

In this paper, we present data showing that pigment-protein complexes tune the vibronic coupling of their chromophores and that the absence of this vibronic coupling activates an oxidative photoprotective mechanism. We use 2DES to show that a pair of cysteine residues in FMO, C49 and C353, can steer excitations toward quenching sites in oxic environments. The measured reaction rate constants demonstrate unusual non-monotonic behavior. We then use a Redfield model to determine how the EET time constants arise from changing chlorophyll site energies and their system-bath couplings(44, 45). The analysis reveals that the cysteine residues tune the

resonance between exciton 4-1 energy gap and an intramolecular chlorophyll vibration in reducing conditions to induce vibronic coupling and detune the resonance in oxidizing conditions. This redox-dependent modulation of the vibronic coupling steers excitations through different pathways in the complex to change the likelihood that they interact with exciton quenchers.

Results

Redox-dependent exciton steering by cysteine residues

We investigate the excitonic pathways that give rise to the different 2DES signals to determine the roles of the cysteine C353 and C49 residues in exciton energy transfer. Two-dimensional electronic spectra map the couplings between excitonic states and show how the couplings evolve over time. The excitation energy (*x*-axis) of the system is correlated with the detection energy (*y*-axis) at each waiting time delay T. We can plot the intensity of peaks in the spectra with increased waiting time to observe the kinetic evolution of the exciton populations. For example, a cross peak below the diagonal can report on energy absorbed at a higher energy state and detected at a lower energy state, indicating energy transfer between these states. **Figure 2** shows 2DES spectra for the FMO wild-type, C353A and C49A single mutants, and C353A/C49A double mutant samples under both oxidizing and reducing conditions at waiting time T=1 ps. At later waiting times, the growth of below diagonal cross peaks, where the excitation energy is greater than the detection energy, indicates that there is downhill EET in the system at sub-picosecond rates. Using averaged time traces for each of these spectra, we extracted the EET time constants for exciton 4-1, 4-2, and 2-1 energy transfer in each sample (see **Figure S1** for overview; see **Supporting Information** for detailed description).

Experimental time constant data in **Table 1** show that the redox environment determines which pathways the excitation energy takes through the complex. Looking first at wild-type FMO under reducing conditions, we see that τ_{41}, τ_{42} and τ_{21} are comparable at 504 ± 12 fs, 408 ± 12 fs, and 455 ± 11 fs, respectively, indicating that exciton 4 is equally likely to transfer energy to exciton 1 through the direct 4-1 or indirect 4-2-1 pathways. The branching ratios representing relative probability of EET for these two pathways are 0.45 and 0.55, respectively(46). When the wild-type FMO is oxidized, τ_{41} gets slower (1.5 ps), τ_{42} gets faster (227 fs), and τ_{21} does not change, indicating that exciton 4 is more likely to transfer energy through the indirect pathway under oxidizing conditions. Under these conditions, the branching ratios for the direct versus indirect pathway become 0.13 and 0.87, respectively. In the 4-2-1 pathway, the excitation is steered to generate higher electron density near the periphery of the system (exciton 2, **Figure 1**). The amino acids near this region contain, among other redox-active residues, a Trp-Tyr chain which has been suggested to play a role in the redox-dependent ultrafast dynamics of the FMO complex(3). Given that τ_{21} does not change, steering the excitation through the 4-2-1 pathway under oxidizing conditions would increase the likelihood of quenching at the cysteine 353 trapping site or charge transfer to the Trp-Tyr chain (**Figure S12**) (43). As shown in previous work (1, 3), we see that the long time signal amplitudes of the oxidized wild-type complex decay faster than those of the reduced wild-type complex. The signal amplitudes of the oxidized wild-type complex also decay faster than those of the C353A/C49A double mutant samples—which decay at similar rates under both redox conditions—indicating that the cysteines are responsible for the observed quenching (**Figure S13**).

Overall, we find that the C353 residue is responsible for exciton steering in reducing conditions, based on the drastic change in time constants in the C353A mutants in reducing conditions. However, we find that both C49 and C353 are active in oxidizing conditions. We observe that the patterns in the time constants are non-monotonic and, in oxidizing conditions, non-

cooperative, as one would expect. A detailed analysis of all single and double mutant EET time constants can be found in the **Supporting Information**.

Redfield model reveals vibronic coupling mechanism for controlling energy transfer

To understand the complex, non-monotonic changes in the time constants for energy transfer as a function of both redox environment and mutation, we employ a Redfield model to show that the FMO protein structure facilitates redox-dependent exciton steering by tuning its resonant coupling with a vibrational mode in bacteriochlorophyll-*a*. The Redfield equation describes the relaxation of an exciton through the excited states of the complex after second order perturbation by the system-bath coupling. The rate of energy transfer increases with the spatial overlap of excitons, resonance between the excitonic energy gap and bath oscillations through the spectral density, and the magnitude of coupling between the system and these bath modes (Huang-Rhys factor) (47, 48). An increased Huang-Rhys factor indicates that there is greater system-bath coupling, meaning that the bath more strongly couples to the excitonic states, and increases the rate of EET (47). Details of the model, our modifications to the parameters, and the approximations made in this model can be found in the **Supporting Information**. We varied the pigment site energies and Huang-Rhys factors for bacteriochlorophyll-*a* sites II, III, and IV. These sites are proximal (within 10 Å) to C353 and C49 and are most likely to be electrostatically perturbed by cysteine mutation and oxidation (20). We use a log-normal spectral density with an added Gaussian curve centered at 260 cm^{-1} representing coupling to a vibrational mode in bacteriochlorophyll-*a (44, 45)*. The most illustrative energy transfer dynamics maps were for sites III and IV, shown in **Figure 3B-D**. The remaining maps can be found in **Figure S3**. In the maps, the *x*-axis represents the relative change in Huang-Rhys factor for a given site, the *y*-axis represents the change in site energy, the colormap represents the value of the energy transfer time constant as a function of these two variables, and the arrows represent changes upon mutation. Our results represent the only consistent set of changes that reproduce the experimental data. The calculated EET time constants can be found in **Table 1**. For example, in **Figure 3B** the dashed blue line pointing downward from 'WT oxidized' to 'oC49A' shows that under oxidizing conditions, mutation of the C49 residue lowers the site III energy by 100 cm^{-1} but does not affect the Huang-Rhys factor, in agreement with the difference in the corresponding calculated time constant in **Table 1**.

Our Redfield model reveals that the FMO protein structure modulates different energy transfer rates by tuning its resonant coupling with the vibrational mode centered at 260 cm^{-1}. **Figure 3A-B** shows that when oxidized or reduced FMO is perturbed by mutation, the energy of site III changes such that the distribution of the exciton 4-1 energy gaps shifts in its resonance with the chlorophyll vibration. When site III energy is raised in this FMO Hamiltonian, the exciton 4-1 energy gap decreases. In the wild-type reduced Hamiltonian, the vibronic coupling between the energy gap distribution and the chlorophyll vibration produces a subpicosecond τ_{41} time constant(23). The oxidized wild-type protein has a 120 cm^{-1} increase in site III energy relative to the reduced wild-type; the slower time constant reflects the fact that the 4-1 energy gap is detuned from the chlorophyll mode (**Figure 3A-B**). In both oxidizing and reducing conditions, we find that the changes to the system Hamiltonian actually represent cooperative effects between mutations, meaning that the changes to the double mutant are a combination of the changes to the two single mutants (**Table 1**).

Generally, the effect of oxidation raises the site III energy based on the number of unmutated cysteines present, while the effect of mutation lowers the site III energy (**Table 1**). Our experimental data showed that τ_{41} slowed down significantly (>5 ps) when the C353 residue was mutated under reducing conditions, discussed above. In the Redfield model, this change is least perturbatively achieved by lowering the energy of site III by >50 cm^{-1}, which increases the 4-1 energy gap and diminishes the vibronic coupling with the chlorophyll mode, as shown by the arrows representing site mutation in **Figure 3B**. The reduced C49A time constants are relatively less changed, so we assume that the site energies for this mutant are roughly equal to the wild-type

reduced parameters. The changes in the reduced double mutant C49A/C353A parameters are thus exclusively caused by the C353A mutation.

In the oxidized samples, mutating C353 or C49 subsequently lowers the site III energy such that the vibronic resonance with the bacteriochlorophyll-*a* mode is increased in each single mutant and is decreased cooperatively in the double mutant. In **Figure 3B**, we see that the calculated τ_{41} time constants in the oxidized single mutants are faster than the double mutant because each single mutant is passing through the resonance vibronic coupling region. These changes to site III upon mutation of the oxidized cysteine residues shift the exciton 4-1 energy gap through various magnitudes of vibronic coupling with the intrinsic chlorophyll mode to facilitate steering of energy transfer pathways.

In the reduced FMO complex, the resonance between the 4-1 energy gap and the spectral density demonstrates that the chlorophyll vibration is able to couple the excitonic states and facilitate energy transfer. The cysteine residues manipulate the electronic Hamiltonian of FMO by tuning the degree of vibronic coupling between the exciton 4-1 energy gap and the intramolecular vibration centered at 260 cm^{-1}. The resulting assignments of site changes to the FMO Hamiltonian are supported within the limitations of Redfield theory because the mutations and redox-conditions primarily perturb the excitonic Hamiltonian – not the system-bath coupling, as evident from the changes in peak position of the linear absorption spectra (**Figure S5**). In this new mechanism, the system steers the excited-state energy transfer toward quenching sites near the protein periphery in response to potentially dangerous oxic conditons.

Discussion

In this study, we show that redox-active residues in FMO steer energy transfer through different pathways in the complex by tuning the excitonic energy in and out of resonance with a vibrational mode of the pigments. In the oxidized wild-type protein and the reduced mutated C353A and C353A/C49A proteins, the vibronic coupling is detuned because the site III energy is changed, causing the exciton 4-1 energy gap to shift out of resonant coupling with an intramolecular vibration in the bacteriochlorophyll molecule. In these conditions, the indirect exciton 4-2-1 energy transfer pathway becomes more kinetically favorable than the direct exciton 4-1 pathway, increasing the likelihood of interacting with quenching sites in the protein. The redox-dependent vibronic coupling shown here exemplifies an evolutionary mechanism by which photosynthetic organisms can exploit the quantum mixing between electronic and vibrational states to control excited state energy transfer dynamics.

Materials and Methods

Experimental Parameters

Two-dimensional spectra of wild-type, C353A, C49A, and C535A/C49A FMO under oxidizing and reducing conditions were acquired at 77 K, as described in detail in a previous publication(3). Briefly, we used a cryostat containing liquid nitrogen (Oxford Instruments) to cool the sample to 77K. To generate a glass, we mixed the protein buffer (CAPS, pH 10.5) with 50% glycerol and loaded the solution into a 200 μm quartz cuvette (Starna) coated with SigmaCote. We generated ‘oxidizing’ conditions by handling the sample in ambient air prior to cooling. To create ‘reducing’ conditions, we added sodium dithionite to a concentration of 10 mM.

For the spectroscopic measurements, using the output of a regenerative amplifier (Coherent Inc. Legend Elite USP, 35 fs, centered at 800 nm), we generated coherent light spanning from 775 to 840 nm via self-phase modulation in 15 psi of argon. The pulse was then temporally compressed to <20 fs using a pulse shaper (Biophotonic Solutions, MIIPS). We acquired 25 2DES spectra for each sample using our single-shot, GRadient Assisted Photon Echo Spectroscopy (GRAPES) setup, described in detail elsewhere(49-52). We also collected pump-probe spectra of

each sample to phase the data using the projection-slice theorem. We phased each spectrum separately and then averaged them to produce an averaged fully absorptive signal.

Extraction of Kinetic Parameters

To obtain the time constants τ_{21}, τ_{42}, and τ_{41} for each FMO sample, we averaged over the diagonal and below diagonal cross peak signals using a circular window with a 70 cm^{-1} range. The center points of the circles for each exciton pair were taken from the peaks of the respective linear absorption spectrum. The signals were then normalized, and the normalized diagonal signals were subtracted from the normalized cross peak signals to remove the bleach recovery contribution. The subtracted signals were then fit to phenomenological kinetic equations for energy transfer. The time constant τ_{21} was fit with the 2 diagonal and 2-1 cross peak, and the τ_{41} and τ_{42} time constants were fit with the 4 diagonal and 4-1 cross peak using the 4 diagonal time constant as a fit constraint.

Redfield Energy Transfer Calculations

We calculated the Redfield energy transfer rates resulting from changing the FMO Hamiltonian. We used the 'Model C' FMO Redfield model developed by Kell *et al.* 2016 (Ref (45)) and their most recent FMO Hamiltonian as listed in Ref (23). Calculated rates using uncorrelated sites were averaged over static disorder with 5,000 Hamiltonians for each site using the same disorder parameters, Huang-Rhys factors, variances, and bath cutoff frequencies as listed in Ref (45). We added a Gaussian line centered at 260 cm^{-1} with a FWHM of 20 cm^{-1} to the spectral density of each site. We calculate the energy rates after varying the site energies and Huang-Rhys factors for sites II, III, and IV. We fit to the set of changes for each FMO sample and constrained the set such that mutation and oxidation are consistent for all FMO samples.

Acknowledgments

This work was supported by the Air Force Office of Scientific Research (AFOSR) (FA9550-18-1-0099), the NSF (under grant no. 1900359), and the DOE Office of Science (under award number DE-SC0020131). This work was supported as part of the Photosynthetic Antenna Research Center (PARC), an Energy Frontier Research Center funded by the U.S. Department of Energy, Office of Science, Office of Basic Energy Sciences under Award Number DE-SC 0001035. This work was also supported in part by the NSF MRSEC grant programs at the University of Chicago (DMR-1420709). J.S.H. acknowledges support from the NSF-GRFP program. S.H.S. R.E.W., and S.C.M. individually acknowledge support from the Department of Defense (DoD), AFOSR, through the National Defense Science and Engineering Graduate (NDSEG) Fellowship Program, 32 CFR 168a. M.A.A. acknowledges support from the Arnold O. Beckman Postdoctoral Fellowship funded by the Arnold and Mabel Beckman Foundation. The authors thank Dr. Karen Watters for scientific editing of the manuscript. The authors thank Prof. Ryszard Jankowiak and Dr. Adam Kell for detailed insight into their Redfield Model "C" and guidance for implementation of the model. The authors also acknowledge Jonathan Fetherolf for detailed discussions. J.S.H thanks members of the UChicago Graduate Recruitment Initiative Team for being a strong self-advocacy and community network.

References

1. G. S. Orf *et al.*, Evidence for a cysteine-mediated mechanism of excitation energy regulation in a photosynthetic antenna complex. *Proceedings of the National Academy of Sciences* **113**, E4486-E4493 (2016).
2. R. Saer *et al.*, Perturbation of bacteriochlorophyll molecules in Fenna–Matthews–Olson protein complexes through mutagenesis of cysteine residues. *Biochimica et Biophysica Acta (BBA) - Bioenergetics* **1857**, 1455-1463 (2016).
3. M. A. Allodi *et al.*, Redox Conditions Affect Ultrafast Exciton Transport in Photosynthetic Pigment–Protein Complexes. *The Journal of Physical Chemistry Letters* **9**, 89-95 (2018).
4. R. E. Fenna, B. W. Matthews, Chlorophyll arrangement in a bacteriochlorophyll protein from Chlorobium limicola. *Nature* **258**, 573-577 (1975).
5. Z. Liu *et al.*, Crystal structure of spinach major light-harvesting complex at 2.72 Å resolution. *Nature* **428**, 287-292 (2004).
6. R. E. Blankenship, *Molecular Mechanisms of Photosynthesis* (Wiley/Blackwell, Chichester, West Sussex, ed. 2nd, 2014).
7. G. S. Orf, R. E. Blankenship, Chlorosome antenna complexes from green photosynthetic bacteria. *Photosynthesis Research* **116**, 315-331 (2013).
8. H. Li, N.-U. Frigaard, D. A. Bryant, [2Fe-2S] Proteins in Chlorosomes: CsmI and CsmJ Participate in Light-Dependent Control of Energy Transfer in Chlorosomes of Chlorobaculum tepidum. *Biochemistry* **52**, 1321-1330 (2013).
9. T. M. Wahlund, C. R. Woese, R. W. Castenholz, M. T. Madigan, A thermophilic green sulfur bacterium from New Zealand hot springs, Chlorobium tepidum sp. nov. *Archives of Microbiology* **156**, 81-90 (1991).
10. T. Brixner *et al.*, Two-dimensional spectroscopy of electronic couplings in photosynthesis. *Nature* **434**, 625-628 (2005).
11. G. S. Engel *et al.*, Evidence for wavelike energy transfer through quantum coherence in photosynthetic systems. *Nature* **446**, 782-786 (2007).
12. M. Mohseni, P. Rebentrost, S. Lloyd, A. Aspuru-Guzik, Environment-assisted quantum walks in photosynthetic energy transfer. *The Journal of Chemical Physics* **129**, 174106 (2008).
13. G. Panitchayangkoon *et al.*, Long-lived quantum coherence in photosynthetic complexes at physiological temperature. *Proceedings of the National Academy of Sciences* **107**, 12766-12770 (2010).
14. E. Thyrhaug, K. Žídek, J. Dostál, D. Bína, D. Zigmantas, Exciton Structure and Energy Transfer in the Fenna–Matthews–Olson Complex. *The Journal of Physical Chemistry Letters* **7**, 1653-1660 (2016).
15. J. Dostál, J. Pšenčík, D. Zigmantas, In situ mapping of the energy flow through the entire photosynthetic apparatus. *Nature Chemistry* **8**, 705 (2016).
16. H.-G. Duan *et al.*, Nature does not rely on long-lived electronic quantum coherence for photosynthetic energy transfer. *Proceedings of the National Academy of Sciences* **114**, 8493-8498 (2017).
17. M. Maiuri, E. E. Ostroumov, R. G. Saer, R. E. Blankenship, G. D. Scholes, Coherent wavepackets in the Fenna–Matthews–Olson complex are robust to excitonic-structure perturbations caused by mutagenesis. *Nature Chemistry* **10**, 177 (2018).
18. E. Thyrhaug *et al.*, Identification and characterization of diverse coherences in the Fenna–Matthews–Olson complex. *Nature Chemistry* **10**, 780-786 (2018).
19. M. L. Chaillet *et al.*, Static Disorder in Excitation Energies of the Fenna–Matthews–Olson Protein: Structure-Based Theory Meets Experiment. *The Journal of Physical Chemistry Letters* **11**, 10306-10314 (2020).
20. J. Wen, H. Zhang, M. L. Gross, R. E. Blankenship, Membrane orientation of the FMO antenna protein from Chlorobaculum tepidum as determined by mass spectrometry-based footprinting. *Proceedings of the National Academy of Sciences* **106**, 6134 (2009).

21. S. I. E. Vulto *et al.*, Exciton Simulations of Optical Spectra of the FMO Complex from the Green Sulfur Bacterium Chlorobium tepidum at 6 K. *The Journal of Physical Chemistry B* **102**, 9577-9582 (1998).
22. J. Adolphs, T. Renger, How Proteins Trigger Excitation Energy Transfer in the FMO Complex of Green Sulfur Bacteria. *Biophysical Journal* **91**, 2778-2797 (2006).
23. A. Khmelnitskiy *et al.*, Energy landscape of the intact and destabilized FMO antennas from C. tepidum and the L122Q mutant: Low temperature spectroscopy and modeling study. *Biochimica et Biophysica Acta (BBA) - Bioenergetics* **1859**, 165-173 (2018).
24. B. S. Rolczynski *et al.*, Correlated Protein Environments Drive Quantum Coherence Lifetimes in Photosynthetic Pigment-Protein Complexes. *Chem* **4**, 138-149 (2018).
25. E. Romero *et al.*, Quantum coherence in photosynthesis for efficient solar-energy conversion. *Nature Physics* **10**, 676-682 (2014).
26. A. W. Chin *et al.*, The role of non-equilibrium vibrational structures in electronic coherence and recoherence in pigment–protein complexes. *Nature Physics* **9**, 113-118 (2013).
27. F. D. Fuller *et al.*, Vibronic coherence in oxygenic photosynthesis. *Nature Chemistry* **6**, 706-711 (2014).
28. J. Cao *et al.*, Quantum biology revisited. *Science Advances* **6**, eaaz4888 (2020).
29. L. Wang, M. A. Allodi, G. S. Engel, Quantum coherences reveal excited-state dynamics in biophysical systems. *Nature Reviews Chemistry* **3**, 477-490 (2019).
30. G. D. Scholes *et al.*, Using coherence to enhance function in chemical and biophysical systems. *Nature* **543**, 647-656 (2017).
31. D. I. G. Bennett, P. Malý, C. Kreisbeck, R. van Grondelle, A. Aspuru-Guzik, Mechanistic Regimes of Vibronic Transport in a Heterodimer and the Design Principle of Incoherent Vibronic Transport in Phycobiliproteins. *The Journal of Physical Chemistry Letters* **9**, 2665-2670 (2018).
32. S. M. Blau, D. I. G. Bennett, C. Kreisbeck, G. D. Scholes, A. Aspuru-Guzik, Local protein solvation drives direct down-conversion in phycobiliprotein PC645 via incoherent vibronic transport. *Proceedings of the National Academy of Sciences* **115**, E3342 (2018).
33. S.-H. Yeh, R. D. Hoehn, M. A. Allodi, G. S. Engel, S. Kais, Elucidation of near-resonance vibronic coherence lifetimes by nonadiabatic electronic-vibrational state character mixing. *Proceedings of the National Academy of Sciences* **116**, 18263 (2019).
34. P. Malý, O. J. G. Somsen, V. I. Novoderezhkin, T. Mančal, R. van Grondelle, The Role of Resonant Vibrations in Electronic Energy Transfer. *ChemPhysChem* **17**, 1356-1368 (2016).
35. M. Z. Papiz, S. M. Prince, T. Howard, R. J. Cogdell, N. W. Isaacs, The Structure and Thermal Motion of the B800–850 LH2 Complex from Rps.acidophila at 2.0Å Resolution and 100K: New Structural Features and Functionally Relevant Motions. *Journal of Molecular Biology* **326**, 1523-1538 (2003).
36. S. J. Harrop *et al.*, Single-residue insertion switches the quaternary structure and exciton states of cryptophyte light-harvesting proteins. *Proceedings of the National Academy of Sciences* **111**, E2666 (2014).
37. H.-Y. S. Chen, M. Liberton, H. B. Pakrasi, D. M. Niedzwiedzki, Reevaluating the mechanism of excitation energy regulation in iron-starved cyanobacteria. *Biochimica et Biophysica Acta (BBA) - Bioenergetics* **1858**, 249-258 (2017).
38. H. Li, S. Jubelirer, A. M. Garcia Costas, N.-U. Frigaard, D. A. Bryant, Multiple antioxidant proteins protect Chlorobaculum tepidum against oxygen and reactive oxygen species. *Archives of Microbiology* **191**, 853 (2009).
39. E. V. Vassilieva *et al.*, Electron Transfer May Occur in the Chlorosome Envelope: The CsmI and CsmJ Proteins of Chlorosomes Are 2Fe-2S Ferredoxins. *Biochemistry* **40**, 464-473 (2001).
40. K. Krumova, G. Cosa, "Chapter 1 Overview of Reactive Oxygen Species" in Singlet Oxygen: Applications in Biosciences and Nanosciences, Volume 1. (The Royal Society of Chemistry, 2016), vol. 1, pp. 1-21.

41. H. B. Gray, J. R. Winkler, The Rise of Radicals in Bioinorganic Chemistry. *Israel Journal of Chemistry* **56**, 640-648 (2016).
42. B. S. Rolczynski, P. Navotnaya, H. R. Sussman, G. S. Engel, Cysteine-mediated mechanism disrupts energy transfer to prevent photooxidation. *Proceedings of the National Academy of Sciences* **113**, 8562 (2016).
43. H. B. Gray, J. R. Winkler, Hole hopping through tyrosine/tryptophan chains protects proteins from oxidative damage. *Proceedings of the National Academy of Sciences* **112**, 10920-10925 (2015).
44. A. Kell, X. Feng, M. Reppert, R. Jankowiak, On the Shape of the Phonon Spectral Density in Photosynthetic Complexes. *The Journal of Physical Chemistry B* **117**, 7317-7323 (2013).
45. A. Kell, R. E. Blankenship, R. Jankowiak, Effect of Spectral Density Shapes on the Excitonic Structure and Dynamics of the Fenna–Matthews–Olson Trimer from Chlorobaculum tepidum. *The Journal of Physical Chemistry A* **120**, 6146-6154 (2016).
46. P. W. Seakins, Product branching ratios in simple gas phase reactions. *Annual Reports Section "C" (Physical Chemistry)* **103**, 173-222 (2007).
47. M. Yang, G. Fleming, Influence of phonons on exciton transfer dynamics : € rster , and modified comparison of the Redfield , F o Redfield equations. **275**, 355-372 (2002).
48. A. Nitzan, *Chemical Dynamics in Condensed Phases: Relaxation, Transfer, And Reactions In Condensed Molecular Systems*, Oxford Graduate Texts (Oxford University Press, ed. 1st, 2014), vol. 1, pp. 742.
49. E. Harel, A. F. Fidler, G. S. Engel, Real-time mapping of electronic structure with single-shot two-dimensional electronic spectroscopy. *Proceedings of the National Academy of Sciences* **107**, 16444-16447 (2010).
50. E. Harel, A. F. Fidler, G. S. Engel, Single-Shot Gradient-Assisted Photon Echo Electronic Spectroscopy. *The Journal of Physical Chemistry A* **115**, 3787-3796 (2011).
51. P. D. Dahlberg *et al.*, Mapping the ultrafast flow of harvested solar energy in living photosynthetic cells. *Nature Communications* **8**, 988 (2017).
52. S. H. Sohail *et al.*, Communication: Broad manifold of excitonic states in light-harvesting complex 1 promotes efficient unidirectional energy transfer in vivo. *The Journal of Chemical Physics* **147**, 131101 (2017).

Figures and Tables

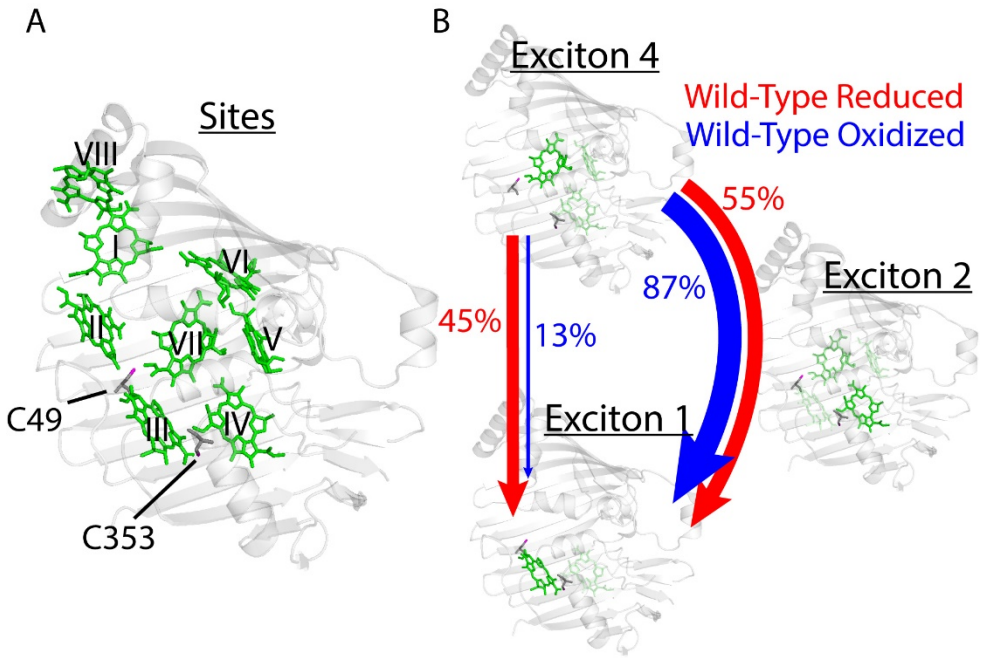

Figure 1. A) Numbered sites and side chains of cysteines C353 and C49 in the FMO pigment-protein complex (PDB: 3ENI)(20). B) Site densities for excitons 4, 2, and 1 in reducing conditions with the energy transfer branching ratios for the wild-type oxidized and reduced protein. The saturation of pigments in each exciton denotes the relative contribution number to the exciton. The C353 residue is located near excitons 4 and 2, which have most electron density along one side of the complex, and other redox active residues such as the Trp/Tyr chain. C353 and C49 surround site III, which contains the majority of exciton 1 density. Excitons 2 and 4 are generally delocalized over sites IV, V, and VII.

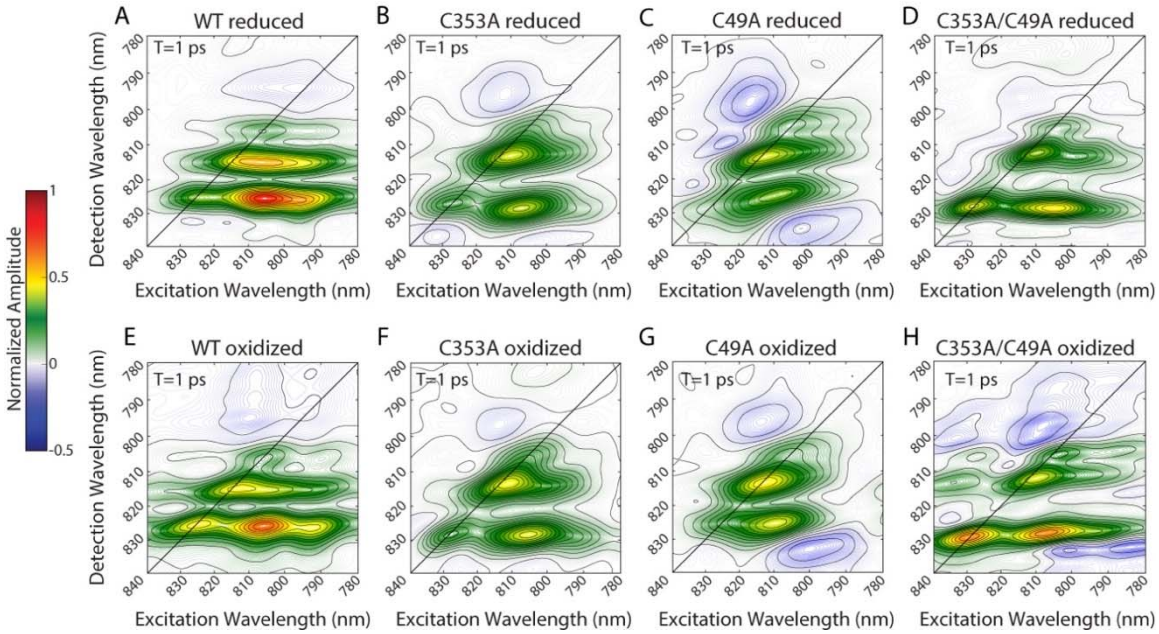

Figure 2. Absorptive 2D spectra of the eight FMO samples at waiting time T=1 ps under reducing (top row, A-D) and oxidizing (bottom row, E-H) conditions. In 2DES, the excitation energy of a system is correlated with the detection energy, and the waiting time T indicates the delay time between the pump and probe pulses. Spectra were normalized to the peak amplitude at time T=0. The three peaks of the diagonal features in each spectrum represent excitons 4, 2, and 1. The growth of cross peaks below the diagonal indicates downhill EET on the timescale of hundreds of femtoseconds.

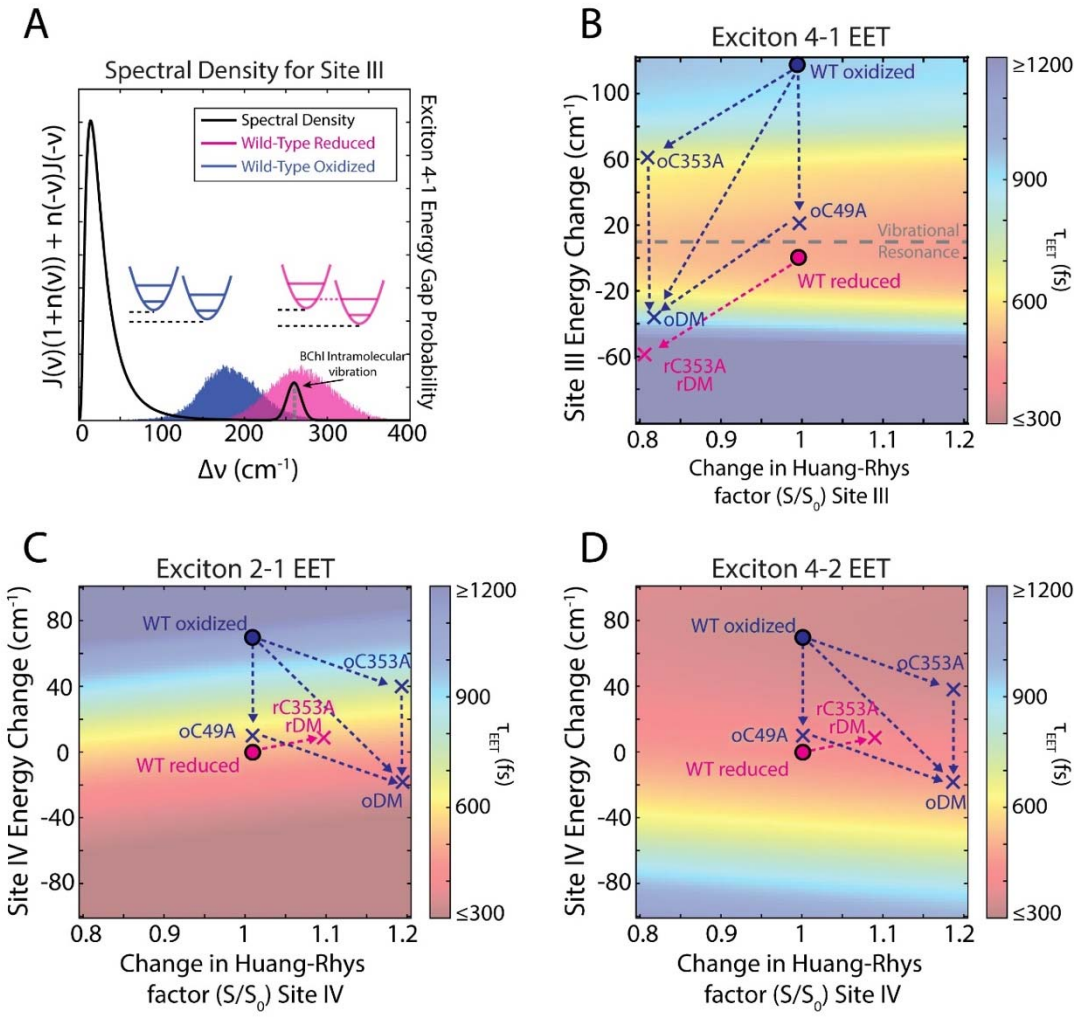

Figure 3. Calculated Redfield energy transfer rates of the FMO Hamiltonian upon changing the site energies and degree of system-bath coupling (Huang-Rhys factors, S) for pigments III (A-B) and IV (C-D). The center points (S/S_0=1; site energy change $\Delta\nu$=0 cm^{-1}; plotted as red circle) represent the wild-type FMO in reducing conditions. The blue circles represent wild-type FMO in oxidizing conditions. **A**) Overlap of the distribution of exciton 4-1 energy gaps in FMO with the spectral density for site III, representing relative vibronic coupling with an intramolecular vibration. Increased overlap with the spectral density indicates that the bath can more readily couple the two excitons, which increases the EET rate. **B**) Change in the τ_{41} time constant as site III energy and Huang-Rhys factor is changed. **C-D**) Change in the τ_{21} and τ_{42} time constants as site IV is changed. The arrows represent how mutation changes each FMO sample. The 'o' and 'r' prefixes represent the oxidized and reduced parameters, respectively. For the reduced FMO samples, there is no change in the C49A parameters, and the C353A changes are the same as the double mutant (DM) changes. In every case, the double mutant is a sum of the two single mutant vectors. The calculated changes in all parameters and the associated energy transfer constants are shown in **Table 1** under 'Redfield Theory'. The same plots but with arrows plotted as oxidation vectors are shown in the Supporting Information.

	Redfield Theory									Experiment		
	Site II change (cm^{-1})	Site III change (cm^{-1})	Site IV change (cm^{-1})	Spectral Density Site II change (S/S_0)	Spectral Density Site III change (S/S_0)	Spectral Density Site IV change (S/S_0)	τ_{21} (fs)	τ_{41} (fs)	τ_{42} (fs)	τ_{21} (fs)	τ_{41} (fs)	τ_{42} (fs)
WT reduced	**0**	**0**	**0**	**1**	**1**	**1**	**508**	**499**	**437**	**455 ± 11**	**504 ± 12**	**408 ± 12**
C353A reduced	0	-60	10	1	0.8	1.1	537	1601	397	544 ± 15	>5000	204 ± 20
C49A reduced	20	0	0	1	1	1	504	535	476	485 ± 13	558 ± 25	537 ± 25
C353A/C49A reduced	20	-60	10	1	0.8	1.1	525	1884	427	567 ± 20	>5000	205 ± 24
WT oxidized	**40**	**120**	**70**	**1**	**1**	**1**	**264**	**1532**	**412**	**439 ± 10**	**1480 ± 11**	**227 ± 11**
C353A oxidized	40	60	40	1	0.8	1.2	395	725	398	438 ± 11	853 ± 14	328 ± 14
C49A oxidized	20	20	10	1	1	1	455	504	443	452 ± 9	520 ± 19	524 ± 19
C353A/C49A oxidized	20	-40	-20	1	0.8	1.2	534	988	509	594 ± 17	1642 ± 21	301 ± 21

Table 1. Calculated changes made to the FMO Hamiltonian to reproduce the general trends in spectroscopic data (left), and experimental energy transfer time constants for wild-type (WT), singly mutated, and doubly mutated FMO samples under reducing and oxidizing conditions extracted from two-dimensional spectra (right). The theoretical time constants were calculated using the 'Model C' Redfield model described in the text. The trends in the time constants calculated with our Redfield model are mapped visually in **Figure 3 and Figure S4**. The experimental time constants were extracted from two-dimensional spectra using the extraction method described in the **Supporting Information**.